

Edge magnetoplasmons in wide armchair graphene ribbons

O. G. Balev,¹ P. Vasilopoulos,² and H. O. Frota¹

¹*Departamento de Física, Universidade Federal do Amazonas, 69077-000, Manaus, Brazil*

²*Department of Physics, Concordia University, 7141 Sherbrooke Ouest, Montréal, Quebec, Canada H4B 1R6*

We show that near an armchair edge of a wide graphene channel, and in the presence of a smooth step-like electrostatic lateral confining potential, the chirality, spectrum, spatial structure, and number of the fundamental edge magnetoplasmons (EMPs), in the $\nu = 2$ regime of the quantum Hall effect, depend strongly on the position of the Fermi level E_F . (i) When E_F is small enough and intersects four degenerate states of the zero Landau level (LL) at one location and two degenerate states of this level at a different one, two fundamental, counter propagating EMPs exist with opposite chirality. This is in contrast with EMPs in conventional two-dimensional electron systems in which only one fundamental EMP exists. For the same wave vector these EMPs have different moduli of phase velocities and an essential spatial overlap. These EMPs can be on resonance in a wide range of frequencies, for micron or submicron lengths along the edge. (ii) When E_F is sufficiently high and intersects only two degenerate states of the zero LL only one fundamental EMP exists with the usual chirality.

PACS numbers: 71.10.Pm, 73.21.-b, 81.05.Uw

I. INTRODUCTION

Since the experimental discovery of graphene and the manifestation of its high-quality free-standing samples¹, graphene has attracted a strong attention, see, e.g., Ref. 2 for recent review. It is currently the subject of many independent studies because its electronic properties are drastically different from those, say, of conventional two-dimensional electron systems (2DES) in semiconductor heterostructures, on liquid helium, etc. Charge carriers in a single-layer graphene behave like "relativistic", chiral massless particles with a "light speed" equal to the Fermi velocity, v_F , and possess a *gapless, linear* spectrum close to the K and K' points¹⁻³. One major consequence is the perfect transmission through arbitrarily high and wide barriers upon normal incidence, referred to as Klein tunneling^{2,4,5}, and the direction-dependent tunneling through barriers⁵. Other unusual properties are a half-integer quantum Hall effect (QHE)^{2,6-8}, a minimum metallic conductivity, and a zitterbewegung^{2,9,10}. The latter effect is due to a lateral confinement of Dirac fermions and its manifestation can be essentially modified by a strong magnetic field^{9,10}. In addition, the submicron long mean-free paths¹ may have important consequences for applications in graphene-based devices, such as transistors, which have already been produced¹¹.

In addition to the aforementioned studies, graphene's edges have also been studied considerably^{2,6-8,12-14}, in particular, in connection with the QHE^{2,6-8}. For some properties it matters whether the edges are of the armchair or zigzag type^{2,6-8}, see Refs. 12,13 for nanoribbons. Also magnetic interface states (that can be understood as a new type of edge states made within a "bulk" of the graphene flake) in graphene-based quantum wires, created by a smooth electrostatic confining potential, have been studied¹⁴. There have also been many studies on plasmons^{15,16} and magnetoplasmons¹⁷, collective wave excitations, in unconfined graphene; for a re-

view on plasmons and magnetoplasmons in conventional 2DES, e.g., see^{18,19}. Different types of edge magnetoplasmons (EMPs) have been studied theoretically^{18,20-27} and experimentally²⁸⁻³⁰ only for conventional 2DESs, see, e.g., Refs.^{18,19}, and in particular Refs.²⁸⁻³⁰ for experimental studies of EMPs in the QHE regime. To our knowledge only the results of the EMP studies of Ref. 24, in the integral QHE regime, explain well the experimental findings of²⁸ and²⁹ for different realistic conditions. Indeed, the classical model of Ref. 18 has major drawbacks in explaining the experimental results in the integer QHE regime, according to the analysis carried out in Ref. 28. This is also the case with the classical model of Ref. 21 according to Refs. 29, 30, and 24.

In this work we explore theoretically the possibility of fundamental EMPs in graphene following Refs. 24,25. As will be shown, in the presence of a smooth yet step-like lateral confining potential near an armchair graphene edge, at $y = L_y/2$, EMPs are possible in the $\nu = 2$ QHE regime. These EMPs depend strongly on the position of the Fermi level E_F . For case (i), referred to in the abstract, the main resonance (Eq. (42), of two EMPs of opposite chirality, localized within a submicron length of an armchair edge) is possible, e.g., if a strong coupling of the EMPs holds at the ends of the segment $L_x^{em} \leq L_x$, where L_x is the length of the graphene channel. Our study shows that the relevant condition $L_x^{em} \lesssim 1\mu\text{m}$ is realistic. The EMPs that we find near a graphene edge are very different from those EMPs treated previously in conventional 2DES, in particular in the integral QHE regime^{18,21-27}.

In Sec. II A we present the wave functions and the spectra of the Landau levels (LLs) in an infinitely large graphene flake in the presence of a perpendicular magnetic field and of a smooth electrostatic confining potential, along the y direction. In Sec. II B we study the combined effect of a smooth, step-like electrostatic confining potential and of armchair graphene edges, at $y = \pm L_y/2$,

on the local Hall conductivity in the $\nu = 2$ QHE regime. In Sec. III we present the resulting EMPs, at an edge region of a wide channel, and their strong dependence on the position of the Fermi level E_F . We make concluding remarks in Sec. IV.

II. GRAPHENE CHANNEL AND LOCAL HALL CONDUCTIVITY

A. Effect of a smooth potential on the LLs

We consider an infinitely large flat graphene flake in the presence of a perpendicular magnetic field $\mathbf{B} = B\hat{z}$ and of a smooth confining potential $V_y = V(y)$ along the y direction, of electrostatic origin. For definiteness we assume that this potential is symmetric. First we consider solutions with energy and wave vector close to the K point. In the nearest-neighbor, tight-binding model the one-electron Dirac Hamiltonian, for massless electrons, is $\mathcal{H} = v_F\vec{\sigma}\cdot\hat{\mathbf{p}} + \mathbb{1}V_y$, with $\mathbb{1}$ the 2×2 unit matrix. Explicitly \mathcal{H} is given by ($e > 0$)

$$\mathcal{H} = v_F \begin{pmatrix} V_y/v_F & p_x - ip_y - eBy \\ p_x + ip_y - eBy & V_y/v_F \end{pmatrix}, \quad (1)$$

where p_x and p_y are the components of the momentum operator \mathbf{p} and $v_F \approx 10^6 m/s$ the Fermi velocity. The vector potential is taken in the Landau gauge, $\mathbf{A} = (-By, 0, 0)$. The equation $(\mathcal{H} - E)\psi = 0$ admits solutions of the form

$$\psi(\mathbf{r}) = e^{ik_x x} \Phi(y) / \sqrt{L_x}, \quad \Phi(y) = \begin{pmatrix} A\Phi_A(y) \\ B\Phi_B(y) \end{pmatrix}, \quad (2)$$

where L_x is the length of the structure along the x axis; due to neglected spin-dependent contributions to the Hamiltonian Eq. (1) each eigenstate is two times degenerated on the spin quantum number. The components $\Phi_A(y)$ and $\Phi_B(y)$ correspond to the two sublattices and are assumed normalized. Then the coefficients A and B satisfy the relation $|A|^2 + |B|^2 = 1$. To simplify the notation in what follows we will write $\Phi_A(y) \equiv \Phi_A$ and $\Phi_B(y) \equiv \Phi_B$. Using Eqs. (1) and (2) we obtain

$$V_y A\Phi_A + \hbar v_F (k_x - y/\ell_0^2 - \partial/\partial y) B\Phi_B = EA\Phi_A, \quad (3)$$

$$\hbar v_F (k_x - y/\ell_0^2 + \partial/\partial y) A\Phi_A + V_y B\Phi_B = EB\Phi_B, \quad (4)$$

where $\ell_0 = (\hbar/eB)^{1/2}$ is the magnetic length. For $E \neq V_y$ we solve Eq. (3) for $A\Phi_A$ and substitute the result in Eq. (4). Assuming $B \neq 0$ and $E - V_y \neq 0$ this gives

$$\left[\frac{\partial^2}{\partial \xi^2} - \xi^2 + \frac{\ell_0^2}{\hbar^2 v_F^2} ((E - U(\xi; y_0))^2 + \frac{\hbar^2 v_F^2}{\ell_0^2}) \right] \Phi_B(\xi) - \frac{d(E - U(\xi; y_0))/d\xi}{E - U(\xi; y_0)} \left(\xi + \frac{\partial}{\partial \xi} \right) \Phi_B(\xi) = 0, \quad (5)$$

where we introduced the dimensionless variable $\xi = (y - y_0)/\ell_0$, with $y_0 = \ell_0^2 k_x$, and the notation $U(\xi; y_0) \equiv V(\ell_0 \xi + y_0) = V(y)$.

Assuming V_y is a smooth function of y , with a characteristic scale $\Delta y \gg \ell_0$, we can make the approximation

$$E - U(\xi; y_0) \approx E - V(y_0) - \xi \frac{\partial U(\xi; y_0)}{\partial \xi} \Big|_{\xi=0}, \quad (6)$$

where it is used that $U(0; y_0) = V(y_0)$.

First, for a given quantum number y_0 , we assume $E = V(y_0)$. Then we rewrite Eq. (5), for $\xi \neq 0$ as

$$\left[\frac{\partial^2}{\partial \xi^2} - \frac{1}{\xi} \frac{d}{d\xi} - \xi^2 (1 - r^2) \right] \Phi_B(\xi) = 0, \quad (7)$$

where $a = \partial U(\xi; y_0)/\partial \xi|_{\xi=0}$ and $r = \ell_0 a / \hbar v_F$. Two independent solutions of Eq. (7) are given by $\xi H_{1/2}^{(1)}(b\xi^2)$ and $\xi H_{1/2}^{(2)}(b\xi^2)$, with $b = (i/2)(1 - r^2)^{1/2}$, where $H_{1/2}^{(1,2)}(z)$ are the Hankel functions. The general solution is a linear combination of them. In particular, for a constant electric field of arbitrary strength, we can obtain exact results for the wave function and eigenvalue of the $n = 0$ LL for both $r < 1$ and $r > 1$, see Refs. 31,32.

For the sake of comparison with the well-known exact results of Refs. 31,32, for a constant electric field and $r < 1$, we first assume $r < 1$. Then we readily obtain $\Phi_B(\xi) \propto \xi H_{1/2}^{(1)}(\xi) \propto \exp[-(1 - r^2)^{1/2} \xi^2/2]$, and

$$A\Phi_A(\xi) = (1/r)[1 + (1/\xi)d/d\xi]B\Phi_B(\xi); \quad (8)$$

it follows that $\Phi_A(\xi) \equiv \Phi_B(\xi)$. So far the calculations were performed for $\xi \neq 0$. Due to $E - U(0; y_0) = 0$, for $\xi = 0$ the transition from Eqs. (3) and (4) to Eqs.(5) and (7) is not yet justified. Here this special point can be dealt with easily because the continuity of the wave function (2) implies that of $\Phi_A(\xi)$ and $\Phi_B(\xi)$ at $\xi = 0$.

The procedure given so far applies to the K valley. If we repeat it for the K' valley, we obtain again Eq. (7). If we label the two valleys by $\kappa = \pm$, we can write both results in the form ($-\infty < \xi < \infty$)

$$\Phi_{A\kappa}(\xi) = \Phi_{B\kappa}(\xi) = [(1 - r^2)/\pi \ell_0^2]^{1/4} e^{-(1 - r^2)^{1/2} \xi^2/2}, \quad (9)$$

$$A_\kappa = (1/r)[1 - \kappa(1 - r^2)^{1/2}]B_\kappa, \quad (10)$$

where $\sqrt{2}A_\kappa = [1 - \kappa(1 - r^2)^{1/2}]^{1/2}$ and $\sqrt{2}B_\kappa = r(1 - \kappa(1 - r^2)^{1/2})^{-1/2}$. For $r \ll 1$ we have $B_+ = A_- \approx 1$ and $A_+ = B_- \approx r/2$. Notice that for the linear potential $V_y = eEy$ the exact results of Refs. 31 and 32 for the $n = 0$ LL coincide with ours, for the eigenvalue $E_{0,k_x} = eEy_0$, and the wave function defined by Eqs. (9), (10). In what follows, we assume that $r \ll 1$.

Now, to study the effect of a smooth potential on the $n \neq 0$ LLs, we will use that for these LLs $|E - V(y_0)| \gg |a|$. Then combining Eq. (6) with Eq. (5) we obtain

$$\left[\frac{\partial^2}{\partial \xi^2} - \xi^2 + \frac{r^2}{a^2} [(E - V(y_0))^2 + \frac{\hbar^2 v_F^2}{\ell_0^2}] \right] \Phi_{B\kappa}(\xi) = 0. \quad (11)$$

This is a harmonic oscillator equation whose solution is standard. For $N = 1, 2, \dots$ the eigenvalues are $E_{\pm N, k_x} = \pm(\hbar v_F/\ell_0)(2N)^{1/2} + V(y_0)$; the eigenfunctions are approximately the well-known ones for $V(y) = 0$. We emphasize that as here $N \neq 0$, the condition $|E - V(y_0)| \gg |a|$ reduces to $r \ll 1$.

Finally, for any $n = 0, \pm 1, \pm 2, \dots$ LL and y_0 not too close to the graphene lattice termination at $y = \pm L_y/2$ (see Fig. 1 which agrees with Ref. 14), the eigenvalues $E_{n, k_x} = E_{n, y_0}$ can be written as

$$E_{n, k_x} = \text{sgn}(n)(\hbar v_F/\ell_0)\sqrt{2|n|} + V(y_0), \quad n = 0, \pm 1, \pm 2, \dots, \quad (12)$$

where the sign function $\text{sgn}(n) = 1$ and -1 for $n > 0$ and $n < 0$, respectively. Notice that each $n \neq 0$ LL is twice degenerate with respect to the valley quantum number κ . Accordingly, for any $n \neq 0$ LL and y_0 not too close to the graphene lattice termination at $y = \pm L_y/2$ (see Figs. 1(a), 1(b), compare with Ref. 14) the eigenvalues (12) are four times degenerate due to the spin and valley degeneracies.

B. Effect of a smooth potential and of an armchair edge on LLs and local Hall conductivity in the $\nu = 2$ QHE regime

Extending magnetotransport formulas for the local Hall conductivity $\sigma_{yx}(y)$ of a standard 2DES in the channel, in the presence of a smooth, lateral confining potential^{33–35}, we obtain, for linear responses and in strong magnetic fields, $\sigma_{yx}(y)$ in the form³⁶

$$\sigma_{yx}(y) = n(y)e/B, \quad (13)$$

where $n(y)$ is the y -dependent electron density given by

$$n(y) = \sum_{\alpha\kappa} f_{\alpha\kappa} \langle \alpha\kappa | \mathbf{1} \delta(\mathbf{r} - \hat{\mathbf{r}}) | \alpha\kappa \rangle, \quad (14)$$

with $\alpha = \{n, k_x\}$. For a finite hole density, $p(y)$, in Eq. (13) it follows that $n(y)$ is changed on $[n(y) - p(y)]$. The standard relation $\sigma_{yx}(y) = -\sigma_{xy}(y)$ holds. Equation (13) can be rewritten as

$$\sigma_{yx}(y) = 2\frac{e^2}{h} \sum_{n \geq 0, \kappa = \pm} \int_{-\infty}^{\infty} dy_0 [f_{n, y_0, \kappa} - \delta_{n, 0} \delta_{\kappa, -}] \times [|A_{\kappa}^n|^2 |\Phi_{A\kappa}^n(\xi)|^2 + |B_{\kappa}^n|^2 |\Phi_{B\kappa}^n(\xi)|^2], \quad (15)$$

with $f_{n, y_0, \kappa}$ the Fermi function and $A_{\kappa}^0, B_{\kappa}^0, \Phi_{A\kappa}^0(\xi), \Phi_{B\kappa}^0(\xi)$ given by Eqs. (10)-(11) in the linear-response limit $r \rightarrow 0$; the factor 2 accounts for spin degeneracy. Point out that $\kappa = \pm$ in Eqs. (14), (15) is actually understood as the pseudospin quantum number; because, at $y_0 > 0$, only for $(L_y/2 - y_0)/\ell_0 \gg 1$ it can be well approximated by the valley index. Indeed, a strong splitting between the electron, $\kappa = +$, and the hole, $\kappa = -$, branches of the $n = 0$ LL^{2,6,14}, due to hybridization of the valley states take place nearby the armchair edge,

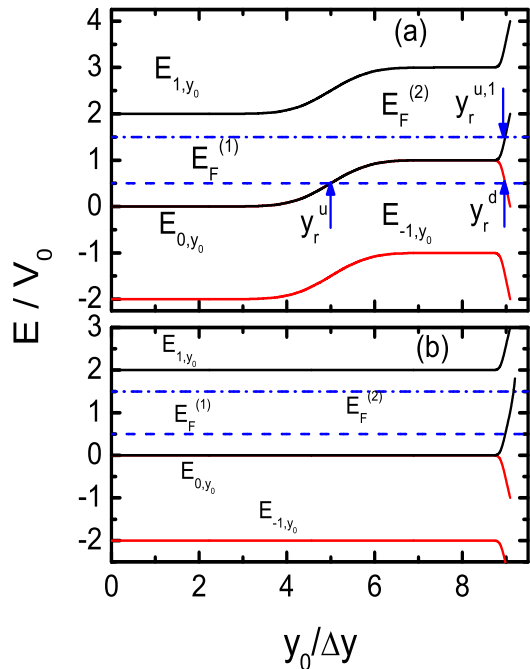


Figure 1: (Color online) (a) Energy spectrum of the $n = -1, 0$, and 1 LLs as a function of the quantum number y_0 , pertinent to the right half of a symmetric graphene channel with armchair edges and the smooth electrostatic potential of finite strength, Eq. (16), for two different values of the Fermi level: (i) $E_F^{(1)} = V_0/2$ and (ii) $E_F^{(2)} = 3V_0/2$. For both cases the $\nu = 2$ quantum Hall effect is manifested in dc magnetotransport; here $V_0 = \hbar v_F/\sqrt{2}\ell_0$, $\Delta y = 10\ell_0$, and ℓ_0 is the magnetic length. In case (i) two spatially separated edge states, of opposite chirality and different degeneracy, are created at $y_r^u = 5\Delta y$ as the four times degenerate $n = 0$ LL crosses the Fermi level $E_F^{(1)}$, and at $y_r^d \approx 9\Delta y$ as the doubly degenerate branch of the $n = 0$ LL crosses $E_F^{(1)}$. Both y_r^u and y_r^d are marked by an upward arrow. In case (ii) only the $n = 0$ LL at $y_r^{u,1} \approx 9\Delta y$ (downward arrow) crosses the Fermi level $E_F^{(2)}$, by its doubly degenerate branch that goes up with increasing y_0 . (b) The same LLs for a graphene channel in the absence of a smooth electrostatic potential; this spectrum agrees with that of Refs. 6–8,13. Here for both positions $E_F^{(1)}$ and $E_F^{(2)}$ of the Fermi level the picture of the edge states is qualitatively the same as case (ii) of Fig. 1a.

at $|L_y/2 - y_0| \leq \ell_0$. The eigenvalues of the $n = 0$ LL for $\kappa = +(-)$ increase (decrease) with increasing y_0 ; in Eq. (15) it is used that the contribution from the $(n = 0, \kappa = -)$ LL is described better by the hole representation. However, for the $n \geq 1$ LLs the $\kappa = \pm$ branches at the armchair edge have a small splitting, due to hybridization of the valley states, as their eigenvalues increase with increasing y_0 ; these branches are attributed to the electron band.

We now consider the situations depicted in Fig. 1(a) for a wide symmetric channel $L_y > 2y_r \gg \Delta y \gg \ell_0$, where $L_y/2 = 9\Delta y$, $y_r/\Delta y = 5$, and $\Delta y/\ell_0 = 10$. However, $y_r/\Delta y$, and $\Delta y/\ell_0$ can take any large value if the EMPs at the right part of the channel are well decoupled

from those at its left part. For clarity the smooth lateral potential is taken as

$$V(y) = (V_0/2) \left[2 + \Phi((y-y_r)/\Delta y) + \Phi((y+y_r)/\Delta y) \right], \quad (16)$$

where $\Phi(x)$ is the probability integral. When the Fermi level E_F is between the bottoms of the $n = 0$ and $n = 1$ LLs, at $y_0 = 0$, and the condition $V_0 \gg 2k_B T$ holds, the occupation of the $n \geq 1$ LLs is negligible; the same holds for the $n = 0$ LL in the regions of y_0 that are well above E_F , see Fig. 1(a). In addition to the smoothness of the potential (16), we assume armchair edges of the graphene sheet at $y = \pm L_y/2$, which cause the bending of the LLs,^{2,6-8,13,14}. In Fig. 1(a) we have $L_y/2 - y_r = 4\Delta y$ but our main results hold qualitatively for $L_y/2 - y_r \gtrsim \Delta y$ as well.

We point out that the fine structure of the LLs $n = \pm 1$ in Figs. 1(a), (b), due to the removal of the pseudospin degeneracy at $|L_y/2 - y_0| \leq \ell_0$ resulting from two possible hybridizations of the valley states for $n \neq 0$ LLs^{6,7}, is discarded. However, a strong splitting of the $n = 0$ LL^{2,6,14} at $|L_y/2 - y_0| \leq \ell_0$, due to only one possible hybridization of the valley states^{6,7}, is taken into account. Due to these assumptions, for y_0 very close to the armchair termination we can formally assume that the eigenvalues in Eq. (15) and the wave functions of the $n \neq 0$ LLs are independent of κ while the eigenvalues of the $n = 0$ LL, for $\kappa = +(-)$ increase (decrease) with increasing y_0 .

For either Fermi level position, $E_F^{(1)}$ or $E_F^{(2)}$ in Fig. 1(a), the $\nu = 2$ quantum Hall regime will be manifested in dc transport measurements. Indeed, for the x axis normal to the plane of Fig. 1(a) and magnetic fields $B > 0$, it follows that at $y_0 = y_r^u$ ($y_r^u = y_r = 5\Delta y$) the fourfold degenerate $n = 0$ LL (composed both of a doubly degenerated conduction band branch, $\kappa = +$, and a doubly degenerated valence band branch, $\kappa = -$) crosses the Fermi level $E_F^{(1)}$ as it goes up, with increasing y_0 . This creates a fourfold degenerate edge state that propagate along the *positive* x axis. However, at $y_0 = y_r^d$ (here $y_r^d \approx 9\Delta y$ is very close to the armchair termination of the graphene channel) only a doubly degenerated valence band branch ($\kappa = -$, with different spin quantum numbers but the same hybridization of the valley states) of the $n = 0$ LL goes down and crosses $E_F^{(1)}$ with increasing y_0 . This branch creates a doubly degenerate edge state that propagate along the *negative* x axis. We call this situation case (i). For the Fermi level position $E_F^{(2)}$ in Fig. 1(a) only a doubly degenerated conduction band branch ($\kappa = +$, with different spin quantum numbers and the same hybridization of the valley states) of the $n = 0$ LL goes up with increasing y_0 and crosses $E_F^{(2)}$ at $y_0 = y_r^{u,1}$, where $y_r^{u,1} \approx 9\Delta y$ is very close to the armchair termination of the graphene channel. This branch creates a doubly degenerate edge state that propagate along the *positive* x axis. We call this situation case (ii).

In Fig. 1(b) we plot the same LLs of the graphene channel in the absence of a smooth electrostatic potential. The spectrum shown is in agreement with that of

Refs. 6–8,13. Here for both $E_F^{(1)}$ and $E_F^{(2)}$ the picture of the edge states is qualitatively the same as that for case (ii) of Fig. 1(a) and magnetotransport measurements will manifest the $\nu = 2$ QHE. Below we show that in cases (i) and (ii) the properties of EMPs are very different.

In case (i), for $y_0 > 0$ and $(y_r^d - y_0)/\ell_0 \gg 1$, from Eqs. (9)-(10), (12), (15) and (16) we obtain

$$\sigma_{yx}(y) = \frac{4e^2}{h} \left[1 + \exp([V(y) - V(y_r^u)]/k_B T) \right]^{-1} - \frac{2e^2}{h}, \quad (17)$$

where it is assumed that $E_{0,y_0} = V(y_0)$ is smooth on the scale of ℓ_0 , i.e., $\ell_0 dV(y_r^u)/dy \ll k_B T$; the factor 4 accounts for spin and pseudospin degeneracy. This condition of smoothness can be rewritten, upon introducing the characteristic length $\ell_T = \ell_0(k_B T/\hbar v_g^u)$, as $\ell_0 \ll \ell_T$, where $v_g^u = \ell_0^{-1} \hbar^{-1} dV(y_r^u)/dy$ is the group velocity at the edge y_r^u . Notice that by using $V_0 = \hbar v_F/\sqrt{2}\ell_0$, $\ell_0/\Delta y = 0.1$, and all other conditions applying to Fig. 1, we obtain $v_g^u = (\ell_0/\sqrt{2\pi}\Delta y) \times v_F \approx 4 \times 10^6$ cm/s. Also, for qualitatively similar conditions we obtain $v_g^u/v_F = (\ell_0/\sqrt{2\pi}\Delta y) \ll 1$ due to the condition $\ell_0/\Delta y \ll 1$.

For sufficiently smooth potentials we can write

$$V(y_r^u + (y - y_r^u)) \approx V(y_r^u) + (y - y_r^u) dV(y)/dy|_{y=y_r^u}, \quad (18)$$

where the second term can be written as

$$(\hbar/\ell_0^2) (y - y_r^u) \frac{dE}{\hbar dk_x}|_{y=y_r^u} = (\hbar/\ell_0^2) v_g^u (y - y_r^u). \quad (19)$$

For $|y - y_r| \leq \ell_T$ the approximation (18) and Eq. (17), for $(\ell_T/\Delta y)^2 \ll 1$, allow us to rewrite Eq. (17) as

$$\sigma_{yx}(y) = \frac{4e^2}{h} \left[1 + \exp[(y - y_r^u)/\ell_T] \right]^{-1} - \frac{2e^2}{h}. \quad (20)$$

We remark that setting $\bar{y} = y - y_r^u$ gives²⁵

$$\frac{d\sigma_{yx}(y)}{dy} = -\frac{4e^2}{h} \frac{1}{4\ell_T \cosh^2(\bar{y}/2\ell_T)}. \quad (21)$$

Hence, in case (i), for $y > 0$ and $(y_r^d - y)/\ell_0 \gg 1$, we have Eqs. (20)-(21). Further, for $L_y/2 \geq y \geq L_y/2 - 5\ell_0$ we model the $\nu = 2$ numerical results^{6,7,13,14} with the density

$$n(y) - p(y) = \frac{1}{\pi^{3/2} \ell_0^3} \int_{-\infty}^{\infty} dy_0 e^{-(y-y_0)^2/\ell_0^2} [f_{0,y_0,-} - 1], \quad (22)$$

where we assumed that $E_{0,y_0,-}$ is a sharply decreasing function at $y_0 \approx y_r^d$ such that the Fermi function in Eq. (22) is very fastly growing at $y_0 \approx y_r^d$ on a scale smaller than ℓ_0 . Then from Eqs. (13) and (22) we obtain

$$d\sigma_{yx}(y)/dy = (2e^2/h\sqrt{\pi}\ell_0) e^{-(y-y_r^d)^2/\ell_0^2}, \quad (23)$$

by changing the derivatives with respect y to those with respect y_0 and integrating by parts.

In a similar manner, for case (ii) and $y > 0$, we obtain that $E_{0,y_0,+}$ is a sharply increasing function at $y_0 \approx y_r^{u,1}$ and

$$d\sigma_{yx}(y)/dy = -(2e^2/h\sqrt{\pi}\ell_0) e^{-(y-y_r^{u,1})^2/\ell_0^2}, \quad (24)$$

in agreement with Fig. 1(a).

III. STRONG DEPENDENCE OF EMPs ON THE FERMI-LEVEL POSITION FOR $\nu = 2$

Now we will study EMPs for cases (i) and (ii), see Fig. 1, neglecting dissipation. We expect that the charge excitation due to EMPs at the right part of channel will be strongly localized at y_r^u ($\rho^{ru}(t, \mathbf{r})$) and y_r^d ($\rho^{rd}(t, \mathbf{r})$), in case (i), and at $y_r^{u,1}$ ($\rho^{r,u1}(t, \mathbf{r})$) in case (ii). Then for case (i) the components of the current density $\mathbf{j}(y)$, in the low-frequency limit $\omega \ll v_F/\ell_0$, are^{24,25}

$$j_x(y) = -\sigma_{yx}E_y(y) + v_g^u \rho^{ru}(\omega, k_x, y) + v_g^d \rho^{rd}(\omega, k_x, y), \quad (25)$$

$$j_y(y) = \sigma_{yx}(y)E_x(y), \quad (26)$$

where we suppressed the factor $\exp[-i(\omega t - k_x x)]$ common to all terms in Eqs. (25) and (26). From Eqs. (25) and (26), Poisson's equation, and the linearized continuity equation we find the integral equation for the charge density $\rho(\omega, k_x, y) = \rho^{ru}(\omega, k_x, y) + \rho^{rd}(\omega, k_x, y)$

$$\begin{aligned} & (\omega - k_x v_g^u) \rho^{ru}(\omega, k_x, y) + (\omega - k_x v_g^d) \rho^{rd}(\omega, k_x, y) \\ & + \frac{2k_x}{\epsilon} \frac{d\sigma_{yx}(y)}{dy} \int_{-\infty}^{\infty} dy' R_g(|y - y'|, k_x; d) \\ & \times [\rho^{ru}(\omega, k_x, y') + \rho^{rd}(\omega, k_x, y')] = 0. \end{aligned} \quad (27)$$

For a metallic gate placed on top of the sample, at a distance d from the 2DES (usually this is a heavily doped Si separated from the graphene sheet by a SiO₂ layer of thickness $d = 300$ nm), $R_g(\dots)$ is given by

$$\begin{aligned} R_g(|y - y'|, k_x; d) &= K_0(|k_x||y - y'|) \\ &- K_0(|k_x|\sqrt{(y - y')^2 + 4d^2}), \end{aligned} \quad (28)$$

where $K_0(x)$ is the modified Bessel function. In the absence of a metallic gate, $d \rightarrow \infty$, the dielectric constant ϵ is spatially homogeneous if not stated otherwise.

As $d\sigma_{yx}(y)/dy$ is too small according to Eqs. (21) and (23) except at $y \approx y_r^u$ and y_r^d , we rewrite Eq. (27) as

$$\begin{aligned} & (\omega - k_x v_g^u) \rho^{ru}(\omega, k_x, y) + (\omega - k_x v_g^d) \rho^{rd}(\omega, k_x, y) \\ & - c_h k_x \left[\frac{1}{2\ell_T \cosh^2(\bar{y}/2\ell_T)} - \frac{1}{\sqrt{\pi}\ell_0} e^{-(y-y_r^d)^2/\ell_0^2} \right] \\ & \times \int_{-\infty}^{\infty} dy' R_g(|y - y'|, k_x; d) \\ & \times [\rho^{ru}(\omega, k_x, y') + \rho^{rd}(\omega, k_x, y')] = 0, \end{aligned} \quad (29)$$

where $c_h = 4e^2/h\epsilon$. In the long-wavelength limit $|k_x|\ell_T \ll 1$ we have $K_0(|k_x(y - y')|) \approx \ln(2/|k_x(y - y')|) - \gamma$, where γ is the Euler constant. The effect of the gate becomes essential if d is not too large, i.e., for $2|k_x|d \lesssim 1$. For the gated sample and $4d^2 \gg \ell_{T,0}^2$, in the long-wavelength limit $2|k_x|d \ll 1$, we have $R_g \approx \ln(2d/|y - y'|)$.

From Eq. (29) it follows that $\rho^{ru}(\omega, k_x, y)$ and $\rho^{rd}(\omega, k_x, y)$ can be well approximated by

$$\rho^{ru}(\omega, k_x, y) = \left[4\ell_T \cosh^2\left(\frac{y - y_r^u}{2\ell_T}\right) \right]^{-1} \rho^{ru}(\omega, k_x), \quad (30)$$

$$\rho^{rd}(\omega, k_x, y) = (1/\sqrt{\pi}\ell_0) e^{-(y-y_r^d)^2/\ell_0^2} \rho^{rd}(\omega, k_x). \quad (31)$$

If we assume $y_r^d - y_r^u \gg \ell_T$, we can neglect any overlap between $\rho^{ru}(\omega, k_x, y)$ and $\rho^{rd}(\omega, k_x, y)$ in Eq. (29). Then, by integration of Eq. (29) over y within separate regions around y_r^u and y_r^d , we obtain two coupled equations for $\rho^{ru}(\omega, k_x)$ and $\rho^{rd}(\omega, k_x)$. They read

$$\begin{aligned} & [(\omega - k_x v_g^u) - 2c_h k_x a_p(k_x; d)] \rho^{ru}(\omega, k_x) \\ & - 2c_h k_x R_g(|y_r^d - y_r^u|, k_x; d) \rho^{rd}(\omega, k_x) = 0, \end{aligned} \quad (32)$$

with $v_g^u = (\ell_0/\sqrt{2\pi}\Delta y)v_F \approx 4 \times 10^6$ cm/s, and

$$\begin{aligned} & [(\omega - k_x v_g^d) + c_h k_x a_m(k_x; d)] \rho^{rd}(\omega, k_x) \\ & + c_h k_x R_g(|y_r^d - y_r^u|, k_x; d) \rho^{ru}(\omega, k_x) = 0, \end{aligned} \quad (33)$$

with $|v_g^d| \gg v_g^u$ and $v_g^d < 0$. Indeed, we estimate a typical $|v_g^d| \sim 3 \times 10^7$ cm/s using numerical results from, e.g., Ref. 13. Notice that from Refs. 31,32 and Sec. II we obtain $|v_g^d| < v_F \approx 10^8$ cm/s; that is, the group velocity of any edge state must be smaller than v_F . The matrix elements $a_p(k_x; d)$ and $a_m(k_x; d)$ are given by

$$a_p(k_x; d) = \frac{1}{16} \int_{-\infty}^{\infty} \int_{-\infty}^{\infty} \frac{dx dt R_g(\ell_T|x - t|, k_x; d)}{\cosh^2(x/2) \cosh^2(t/2)}, \quad (34)$$

$$a_m(k_x; d) = \frac{1}{\pi} \int_{-\infty}^{\infty} \int_{-\infty}^{\infty} \frac{dx dt}{e^{x^2+t^2}} R_g(\ell_0|x - t|, k_x; d). \quad (35)$$

For $|k_x(y_r^d - y_r^u)| \gg 1$ it's a good approximation to neglect the terms $\propto R_g(\dots)$ in Eqs. (32) and (33). Then Eqs. (32) and (33) are decoupled. The resulting dispersion relations for the two fundamental EMP modes are

$$\omega_{+,0}^{(i)}(k_x, d) = k_x v_g^u + 2c_h k_x a_p(k_x; d), \quad (36)$$

for the mode localized at y_r^u , that has *positive* phase and group velocities, and

$$\omega_{-,0}^{(i)}(k_x, d) = -k_x |v_g^d| - c_h k_x a_m(k_x; d), \quad (37)$$

for the mode localized at y_r^d that has *negative* phase and group velocities. Notice that in the long-wavelength limit and for large d the effect of the gate, $\propto \exp(-2|k_x|d) \ll 1$,

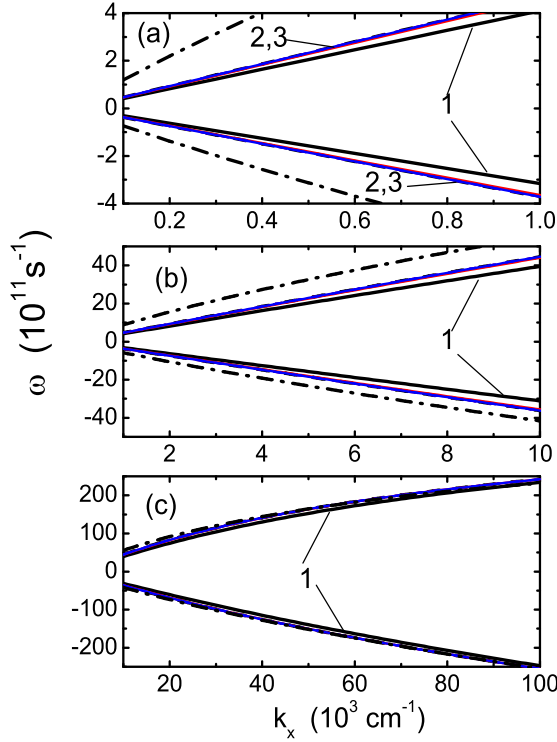


Figure 2: (Color online) The dispersion relations $\omega_{\pm}^{(i)}(k_x, d = 300 \text{ nm})$ (solid curves), $\omega_{\pm,0}^{(i)}(k_x, d = 300 \text{ nm})$ (dashed curves), and $\omega_{\pm,0}^{(i)}(k_x, d \rightarrow \infty)$ (dot-dashed curves) of two counter-propagating fundamental EMPs for case (i) at $\nu = 2$. Panels (a), (b), and (c) correspond to three characteristic k_x regions: $10^3 \text{ cm}^{-1} \geq k_x \geq 10^2 \text{ cm}^{-1}$ in (a), $10^4 \text{ cm}^{-1} \geq k_x \geq 10^3 \text{ cm}^{-1}$ in (b), and $10^5 \text{ cm}^{-1} \geq k_x \geq 10^4 \text{ cm}^{-1}$ in (c). The solid curves marked by 1, 2, and 3 correspond, respectively, to inter-edge distances, in the $n = 0$ LL, $y_r^d - y_r^u = \Delta y$, $4\Delta y$, and $16\Delta y$. The other parameters are $B = 9T$, $T = 77\text{K}$, $\ell_T/\ell_0 = 2$, $\Delta y = 10\ell_0$, $v_g^u = 4 \times 10^6 \text{ cm/s}$, $v_g^d = -3 \times 10^7 \text{ cm/s}$, $\epsilon = 2$, and $\ell_0 \approx 8.5 \text{ nm}$.

can be neglected in Eqs. (36) and (37). The result is $a_p(k_x; d) \rightarrow [\ln(1/|k_x|\ell_T) - 0.145]$ and $a_m(k_x; d) \rightarrow [\ln(1/|k_x|\ell_0) + 3/4]$.

For case (ii), in the low-frequency limit $\omega \ll v_F/\ell_0$, the result is

$$\rho^{r,u1}(\omega, k_x, y) = \frac{1}{\sqrt{\pi}\ell_0} e^{-(y-y_r^{u,1})^2/\ell_0^2} \rho^{r,u1}(\omega, k_x). \quad (38)$$

Using Eq. (24) and other relevant expressions gives, for $\rho^{r,u1}(\omega, k_x) \neq 0$, the dispersion relation for only one fundamental EMP mode, localized mainly at $y_r^{u,1}$,

$$\omega^{(ii)}(k_x, d) = k_x v_g^{u1} + c_h k_x a_m(k_x; d), \quad (39)$$

with *positive* phase and group velocities. Here $v_g^{u1} > 0$ and, similar to $|v_g^d|$, we estimate $v_g^{u1} \lesssim 3 \times 10^7 \text{ cm/s}$.

If we take into account the coupling in Eqs. (32)-(33), due to $R_g(|y_r^d - y_r^u|, k_x; d) \neq 0$, then a nontrivial solution of this system requires its determinant to vanish. This

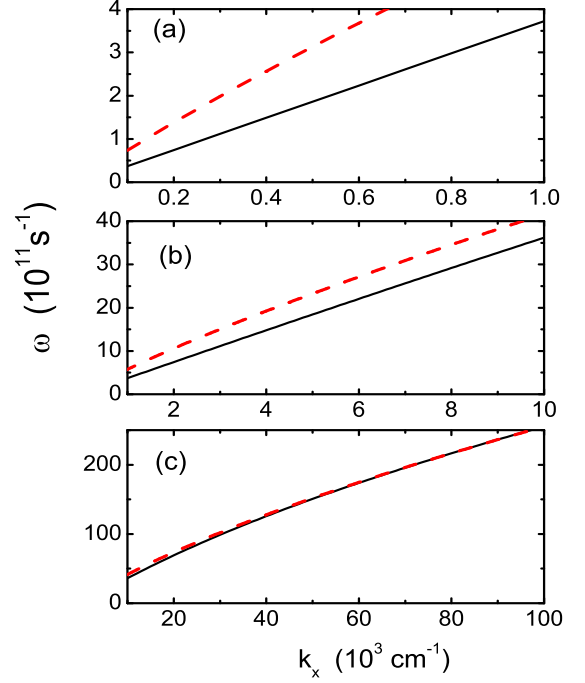


Figure 3: (Color online) The dispersion relations of the unique, left fundamental EMP for case (ii) and two values of d , $\omega_{\pm}^{(ii)}(k_x, d = 300 \text{ nm})$ (solid curves), and $\omega_{\pm}^{(ii)}(k_x, d = \infty)$ (dashed curves). Panels (a), (b), and (c) correspond, respectively, to panels (a), (b), and (c) of Fig. 2. Here $v_g^{u1} = 3 \times 10^7 \text{ cm/s}$ and the other parameters are the same as those in Fig. 2.

leads to two renormalized EMP modes, $\omega_+^{(i)}$ and $\omega_-^{(i)}$,

$$\begin{aligned} \omega_{\pm}^{(i)}(k_x, d) &= \frac{1}{2} \left[\omega_{+,0}^{(i)}(k_x, d) + \omega_{-,0}^{(i)}(k_x, d) \right] \\ &\pm \frac{1}{2} \left[\left[\omega_{+,0}^{(i)}(k_x, d) - \omega_{-,0}^{(i)}(k_x, d) \right]^2 \right. \\ &\left. - 8c_h^2 k_x^2 R_g^2(y_r^d - y_r^u, k_x; d) \right]^{1/2}, \end{aligned} \quad (40)$$

where $\omega_{\pm,0}^{(i)}(k_x, d)$ are given by Eqs. (36)-(37). If we neglect the Coulomb coupling $R_g(\dots)$ between the charge excitations at y_r^d and y_r^u , Eq. (40) leads to the limits $\omega_+^{(i)}(k_x, d) \rightarrow \omega_{+,0}^{(i)}(k_x, d)$ and $\omega_-^{(i)}(k_x, d) \rightarrow \omega_{-,0}^{(i)}(k_x, d)$.

From Eqs. (40) and (32)-(33) it follows that

$$\begin{aligned} \rho^{ru}(\omega_+^{(i)}(k_x, d), k_x) / \rho^{rd}(\omega_+^{(i)}(k_x, d), k_x) \\ = 2\rho^{rd}(\omega_-^{(i)}(k_x, d), k_x) / \rho^{ru}(\omega_-^{(i)}(k_x, d), k_x), \end{aligned} \quad (41)$$

for any d , $y_r^d - y_r^u$, and k_x , in particular for $d \rightarrow \infty$. That is, the ratio of the charge amplitudes $\rho^{ru}(\omega_+^{(i)}(k_x, d), k_x) / \rho^{rd}(\omega_+^{(i)}(k_x, d), k_x) \equiv \rho_+^{ru} / \rho_+^{rd}$ for the $\omega_+^{(i)}(k_x, d)$ EMP, at the edges y_r^u and y_r^d , times the ratio $\rho_-^{ru} / \rho_-^{rd}$, for the $\omega_-^{(i)}(k_x, d)$ EMP, is equal to 2.

For case (i) and $\nu = 2$, in Fig. 2 we plot the dispersion relations $\omega_{\pm}^{(i)}(k_x, d = 300 \text{ nm})$ (solid curves, Eq. (40)), $\omega_{\pm,0}^{(i)}(k_x, d = 300 \text{ nm})$ (dashed curves, Eqs.

(36)-(37)), and $\omega_{\pm,0}^{(i)}(k_x, d \rightarrow \infty)$ (dot-dashed curves) for $v_g^u = 4 \times 10^6$ cm/s, $v_g^d = -3 \times 10^7$ cm/s, and $\epsilon = 2$, in three characteristic k_x regions: $10^3 \text{ cm}^{-1} \geq k_x \geq 10^2 \text{ cm}^{-1}$ in (a), $10^4 \text{ cm}^{-1} \geq k_x \geq 10^3 \text{ cm}^{-1}$ in (b), and $10^5 \text{ cm}^{-1} \geq k_x \geq 10^4 \text{ cm}^{-1}$ in (c). Here we assume that on one side of the graphene sheet there is SiO_2 substrate, with dielectric constant ≈ 3 , and on the other side there is air or vacuum: then for ϵ we must use, in all formulas, an effective dielectric constant ≈ 2 . The other parameters used are $B = 9\text{T}$, $T = 77\text{K}$, $\Delta y = 10\ell_0$, which gives $\ell_T/\ell_0 = 2$, and $\ell_0 \approx 8.5$ nm. The solid curves marked by 1, 2, and 3 correspond to the inter-edge distance of the $n = 0$ LL $y_r^d - y_r^u = \Delta y$, $4\Delta y$, and $16\Delta y$, respectively. For any of these curves we assume $(y_r^d - y_r^u)/y_r^d \ll 1$; the dashed and dot-dashed curves are independent of the inter-edge distance. This allows us to neglect the coupling of the fundamental EMPs, localized in some regions of $y > 0$, with any EMPs on the left part of channel. In particular, for $y_r^d - y_r^u = 16\Delta y$ the channel width is much larger than that used in Fig. 1. The solid curves 1, 2, and 3 are very close in (a) to pertinent dashed curve and are even closer in (b) and (c). Resonances due to these two counter propagating EMPs (localized in a region of extent $\leq 1\mu\text{m}$, from the right edge at $y \approx y_r^d$) are possible in (a),(b), and (c) for $L_x \sim 10^{-2}\text{cm}$, $\sim 10^{-3}\text{cm}$, and $\sim 10^{-4}\text{cm}$, respectively. In Fig. 2(a) the solid and dashed curves show a strong effect of the gate, compare with the dot-dashed curves, and their behavior is very close to a linear one. In Fig. 2(c) both the effect of the gate and that of $y_r^d - y_r^u$ become essentially smaller for the curves 1, 2, and 3.

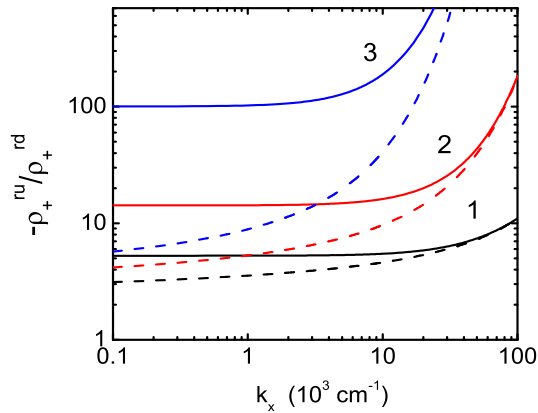


Figure 4: (Color online) The ratio $-\rho_+^{ru}/\rho_+^{rd} = -2\rho_+^{rd}/\rho_+^{ru}$ versus k_x for case (i), $\nu = 2$, and other conditions as in Fig. 2. The solid (dashed) curves correspond to $d = 300$ nm ($d \rightarrow \infty$). The curves 1, 2, and 3 correspond to $y_r^d - y_r^u = \Delta y$, $4\Delta y$, and $16\Delta y$, respectively, and $\Delta y = 10\ell_0$.

For case (ii) and $\nu = 2$ in Fig. 3 we plot the dispersion relations of the unique left fundamental EMP $\omega^{(ii)}(k_x, d)$, Eq. (39), for two characteristic values of d , $d = 300$ nm (solid curves) and $d = \infty$ (dashed curves), and the same three characteristic k_x regions of Fig. 2.

In Fig. 4, for case (i) and other conditions as in Fig. 2, we plot the ratio $-\rho_+^{ru}/\rho_+^{rd}$ versus k_x . The curves

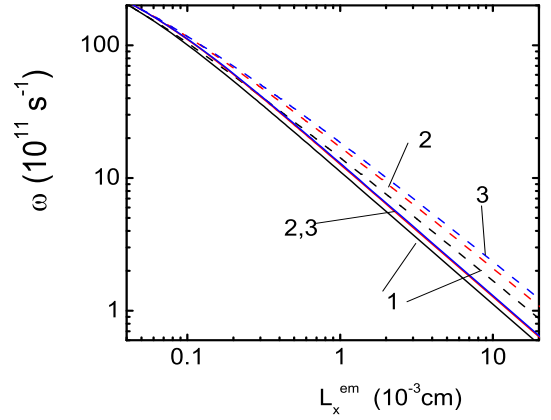


Figure 5: (Color online) The main resonance frequency ω as function of L_x^{em} , calculated from Eq. (42) with $N = 1$, for case (i), $\nu = 2$, and other conditions as in Fig. 2. The resonance is due to two counter propagating fundamental EMPs, Eq. (40), localized between the edge states, at y_r^u and y_r^d , of the $n = 0$ LL. The solid (dashed) curves correspond to $d = 300$ nm ($d \rightarrow \infty$). The curves 1, 2, and 3 correspond to $y_r^d - y_r^u = \Delta y$, $4\Delta y$, and $16\Delta y$, respectively, $\Delta y = 10\ell_0$, and $\ell_0 = 8.5$ nm.

1, 2, and 3 are obtained from Eqs. (32), (40)-(41). The solid curves correspond to $d = 300$ nm and the dashed ones to $d \rightarrow \infty$. According to Eq. (41) we have $\rho_+^{ru}/\rho_+^{rd} = 2\rho_+^{rd}/\rho_+^{ru}$. Figure 4 shows that the fundamental EMPs with positive ($\omega_+^{(i)}(k_x, d)/k_x > 0$), and negative phase velocity ($\omega_-^{(i)}(k_x, d)/k_x < 0$), renormalized by the inter-edge Coulomb interaction, have their charge density amplitudes, at different edges (i.e., at y_r^u and y_r^d), in opposite phase. Moreover, for the former EMP the charge excitation is mainly localized at the edge y_r^u (i.e., the position of edge states due to the smooth confining potential) as $-\rho_+^{ru}/\rho_+^{rd} > 1$, whereas for the latter EMP it is mainly localized at the edge y_r^d as $-\rho_+^{ru}/\rho_+^{rd} < 1$.

In Fig. 5, for case (i) and other conditions as in Fig. 2, we plot the main resonance, at $N = 1$, obtained for the $\omega_{\pm}^{(i)}(k_x, d)$ EMPs from

$$[k_x^+(\omega) - k_x^-(\omega)] L_x^{em} = 2\pi N, \quad (42)$$

where L_x^{em} is the length of a segment of the right edge along which the EMPs propagate freely, see Eq. (40). Due to the counter propagation of these two EMPs, the relation $L_x^{em} \leq L_x$ is possible. In particular, we will have $L_x^{em} \ll L_x$ if a strong coupling between the EMPs, Eq. (40), is introduced in the relevant high-frequency range within two spatial regions separated by $L_x^{em} \ll L_x$, along the right graphene edge(s). Actually, as we see, e.g., in Fig. 1(a) the right edge in case (i) consists of two edges, at y_r^u and y_r^d , with pertinent edge states (due to two intersections of the $n = 0$ LL with the Fermi level). Despite that y_r^d is very close to the right armchair termination of the channel, it follows that $L_y/2 > y_r^d$. In Eq. (42) the EMP's wave vector $k_x^{\pm}(\omega)$ is obtained from Eq. (40) abbreviated as $\omega = \omega_{\pm}^{(i)}(k_x^{\pm}, d)$.

In addition, for case (i) a strong Bragg coupling is possible due to a weak superlattice along the edge, with period L_x^{em} , if $L_x/L_x^{em} \gg 1$. In particular, for frequencies in the THz range, see Fig. 5, $L_x^{em} \lesssim 1\mu\text{m}$ and $L_x/L_x^{em} \gtrsim 10^2$ correspond to rather typical lengths $L_x \gtrsim 10^2 \mu\text{m}$ in experiments.

IV. CONCLUDING REMARKS

We studied EMPs near an armchair edge of a wide graphene channel, at $y = L_y/2$, with a smooth lateral potential, in the $\nu = 2$ regime of QHE and when the Fermi level E_F is in a gap. We showed that the position of E_F can strongly affect the chirality, spectrum, spatial structure, and the number of the fundamental EMPs. When $E_F^{(1)}$ intersects four degenerate states of the $n = 0$ LL at $y_r^u > 0$ and two degenerate states of this level at $y_r^d \gg y_r^u - y_r^u \gg \ell_0$ (case (i)), two fundamental EMPs, with opposite chirality, counter propagate along the right edge of the channel. For the same wave vector the absolute values of their phase velocities are different and they have spatial structure along the y axis, with an essential overlap in the region between the edge states, at y_r^u and y_r^d , and their vicinity. That is, the right edge consists of two edges at y_r^u and y_r^d , with pertinent edge states, due to the $n = 0$ LL. When the Fermi level is sufficiently high, $E_F^{(2)}$, and intersects only two degenerate states of the $n = 0$ LL at $y_r^{u,1} \approx y_r^d$ (case (ii)), only one fundamental EMP exists, of the "usual" chirality for edges of n type conventional 2DES.

In case (i) we found that a resonance of two fundamental EMPs, of opposite chirality, on the (right) edge of a graphene channel, is possible in a wide region of frequencies. The main resonance described by Eq. (42) is allowed in segment lengths $L_x^{em} \leq L_x$ along the edge. The $N = 1$ resonance means that the sum of the total increases of the wave phases of the $\omega_+^{(i)}(k_x, d)$ and $\omega_-^{(i)}(k_x, d)$ EMPs, during their propagation between the ends of L_x^{em} along the positive and negative x axis, respectively, is equal to 2π . This partly resembles the condition for the main resonance of a usual EMP, see, e.g., Ref.^{18,20}, where the EMP propagating along the perimeter P of a conventional 2DES, typically $P \gtrsim 10^{-1}\text{cm}$ ^{18,20,24}, acquires a phase 2π . Moreover, for experimentally realistic values of L_x we obtained $L_x^{em} \ll L_x$. Indeed, for frequencies in the THz range and $L_x^{em} \lesssim 1\mu\text{m}$ the experimentally realistic values $L_x \sim 10^2 \mu\text{m}$ entail $L_x/L_x^{em} \geq 10^2$. Then we can speculate that a strong Bragg coupling is possible due to a weak periodic superlattice along the edge with period L_x^{em} . Notice that a weak superlattice potential along the edge, with period $\gtrsim 10^2 \text{nm}$, has negligible effect on a fundamental EMP in the QHE regime in conventional 2DESs²⁷. In addition, as two renormalized fundamental EMP modes $\omega_{\pm}^{(i)}$, Eq. (40), are counter propagating and their spatial structures have essential overlap along y , in

a narrow region between y_r^u and y_r^d , that can easily be modified due to the strong dependence of y_r^u on a smooth lateral electrostatic potential, time-resolved experiments, such as those of Refs. 28,29, can be used to observe appearance of counter propagating EMP along the armchair edge in the $\nu = 2$ QHE regime. As far as, shown in Fig. 1(a), case (i) is realized, that can be realized for a wide range of parameters. The entire EMP picture and properties are different from those of EMPs in conventional 2DESs due to the difference in the spectrum of the edges and the corresponding wave functions. In fact, as was mentioned earlier in Fig. 1(b) and above Eq. (17), in the absence of a smooth electrostatic potential the spectrum agrees with the usual, hard-wall potential of Refs. 6–8,13. Correspondingly, we don't have two counterpropagating fundamental EMPs but only one fundamental EMP with properties similar to those of the fundamental EMP in conventional 2DES.

Next we list and discuss the approximations used. In studying the EMPs in the $\nu = 2$ QHE regime we neglected dissipation. This approximation is well justified as the EMP damping can be related only with inelastic scattering processes within narrow temperature belts, of width $k_B T$, of each edge state, cf.^{24,25}, that are much weaker than scattering processes due to a static disorder, especially in the QHE regime which implies relatively low T . The latter makes a dominant contribution to the transport scattering time in a 2DES of graphene^{1,2,37} for $B = 0$. Further, the damping of the EMPs will influence some properties of a Bragg coupling and the quality of the EMP resonances, cf. Eq. (42). Notice that for decreasing temperature T any EMP damping will quickly weaken. However, for sufficiently small T the condition $\ell_T/\ell_0 \gg 1$ can be violated. Nevertheless, at quite low T and for sufficiently smooth bare confining potential, the group velocity can essentially decrease with decreasing temperature²⁵ due to many-body effects. In addition, even for $\ell_T/\ell_0 \ll 1$ it appears that the present results will be only weakly and quantitatively modified since the contributions to a fundamental EMP coming from a region of the LL edge, at y_r^u , will bring about only small changes^{24–26}. Obviously, for a more accurate account of the EMPs studied here dissipation must be included in the treatment. We emphasize that our study of the fundamental EMPs for the armchair termination of a graphene channel cannot be directly extended to zigzag termination as some important properties of the wave functions and the energy levels are different than those of the armchair termination, cf.^{2,6–8,13}. We relegate the study of EMPs along zigzag edges to a future work.

We used a simple analytical model of a smooth, lateral confining potential Eq. (16), but our main results are quite robust to modifications of its form and parameters since cases (i) and (ii) can be realized in a graphene channel in the $\nu = 2$ QHE regime. Further, near the edge states at y_r^d and $y_r^{u,1}$ we used a simple analytic model to approximate a static density profile, cf. Eq. (22). In doing so we neglected possible modifications

of the static density profile due to local charging^{34,38,39} $\propto d^2V(y)/dy^2$. Notice that these modifications are weak for a smooth potential and their neglect should have a minor effect in the fundamental EMPs we studied as their main properties are very robust against details of a static density profile^{24–26} and, in particular, nonlocal effects²⁶.

Acknowledgments

This work was supported by the Brazilian Council for Research (CNPq) APV Grant No. 452849/2009-8

and the Canadian NSERC Grant No. OGP0121756, O. G. B. also acknowledges support by Brazilian FAPEAM (Fundação de Amparo à Pesquisa do Estado do Amazonas) Grant.

-
- ¹ K. S. Novoselov, A. K. Geim, S. V. Morozov, D. Jiang, Y. Zhang, S. V. Dubonos, I. V. Grigorieva, and A. A. Firsov, *Science* **306**, 666 (2004); K. S. Novoselov, *Proc. Natl. Acad. Sci. USA* **102**, 10451 (2005); A. K. Geim and K. S. Novoselov, *Nature Materials*, **6**, 183 (2007).
- ² A. H. Castro Neto, F. Guinea, N. M. R. Peres, K. S. Novoselov, and A. K. Geim, *Rev. Mod. Phys.* **81**, 109 (2009).
- ³ P. R. Wallace, *Phys. Rev.* **71**, 622 (1947).
- ⁴ O. Klein, *Z. Phys.* **53**, 157 (1929).
- ⁵ M. I. Katsnelson, K. S. Novoselov, A. K. Geim, *Nature Phys.* **2**, 620 (2006); J. Milton Pereira Jr., P. Vasilopoulos, and F. M. Peeters, *Appl. Phys. Lett.* **90**, 132122, (2007).
- ⁶ L. Brey and H. A. Fertig, *Phys. Rev. B* **73**, 195408 (2006); N. M. R. Peres, F. Guinea, A. H. Castro Neto, *ibid* **73**, 125411 (2006).
- ⁷ D. A. Abanin, P. A. Lee, and L. S. Levitov, *Phys. Rev. Lett.* **96**, 176803 (2006); *Solid State Commun.*, **143**, 77 (2007).
- ⁸ V. P. Gusynin, V. A. Miransky, S. G. Sharapov, and I. A. Shovkovy, *Phys. Rev. B* **77**, 205409 (2008).
- ⁹ N. M. R. Peres, A. H. Castro Neto, F. Guinea, *Phys. Rev. B* **73**, 241403 (2006).
- ¹⁰ H.-Y. Chen, V. Apalkov, and T. Chakraborty, *Phys. Rev. Lett.* **98**, 186803 (2007); A. V. Shytov, M. S. Rudner, and L. S. Levitov, *ibid* **101**, 156804 (2008).
- ¹¹ L. A. Ponomarenko *et al.*, *Science* **320**, 356 (2008); C. Stampfer, E. Schurtenberger, F. Molitor, J. Guttinger, T. Ihn, and K. Ensslin, *Nano Lett.* **8**, 2378 (2009).
- ¹² B. Trauzettel Denis V. Bulaev, D. Loss, and G. Burkard, *Nature Phys.* **3**, 192 (2007); K. Nakada, M. Fujita, G. Dresselhaus, and M. S. Dresselhaus, *Phys. Rev. B* **54**, 17954 (1996).
- ¹³ V. P. Gusynin, V. A. Miransky, S. G. Sharapov, I. A. Shovkovy, and C. M. Wyenberg, *Phys. Rev. B* **79**, 115431 (2009).
- ¹⁴ J.M. Pereira, F. M. Peeters, and P. Vasilopoulos, *Phys. Rev. B* **75**, 125433 (2007).
- ¹⁵ S. Das Sarma and E. H. Hwang, *Phys. Rev. Lett.* **102**, 206412 (2009); M. Polini, R. Asgari, G. Borghi, Y. Barlas, T. Pereg-Barnea, and A. H. MacDonald, *Phys. Rev. B* **77**, 081411(R) (2008); Yu Liu, R. F. Willis, K. V. Emtsev, and Th. Seyller, *ibid* **78**, 201403(R) (2008).
- ¹⁶ B. Wunsch, T. Stauber, F. Sols, and F. Guinea, *New J. Phys.* **8**, 318 (2006); X. F. Wang and T. Chakraborty, *Phys. Rev. B* **75**, 033408 (2007); T. Langer, J. Baringhaus, H. Pfner, H. W. Schumacher, and C. Tegenkamp, *New J. Phys.* **12**, 033017 (2010).
- ¹⁷ O. L. Birman, G. Gumbs, and Y. E. Lozovik, *Phys. Rev. B* **78**, 085401 (2008); R. Roldan, J.-N. Fuchs, and M. O. Goerbig, *ibid* **80** 085408 (2009); Yu. A. Bychkov and G. Martinez, *ibid* **77** 125417 (2008); A. Iyengar, J. Wang, H. A. Fertig, and L. Brey, *ibid* **75** 125430 (2007).
- ¹⁸ V.A. Volkov and S.A. Mikhailov, “Electrodynamics of Two-Dimensional Electron Systems in High Magnetic Fields,” in *Landau Level Spectroscopy, Modern Problems in Condensed Matter Sciences*, Ed. by G. Landwehr and E. I. Rashba (North-Holland, Amsterdam, 1991), vol. 27.2, ch.15, p. 855-907; V.A. Volkov and S.A. Mikhailov, *Zh. Eksp. Teor. Fiz.* **94**, 217 (1988) [*Sov. Phys. JETP* **67**, 1639 (1988)].
- ¹⁹ M.S. Kushwaha, *Surface Science Reports* **41**, p. 1-416 (2001).
- ²⁰ A. L. Fetter, *Phys. Rev. B* **32**, 7676 (1985); V. A. Volkov and S. A. Mikhailov, *Pis'ma Zh. Eksp. Teor. Fiz.* **42**, 450 (1985) [*JETP Lett.* **42**, 556 (1985)].
- ²¹ I. L. Aleiner and L. I. Glazman, *Phys. Rev. Lett.* **72**, 2935 (1994).
- ²² B. I. Halperin, *Phys. Rev. B* **25**, 2185 (1982); X. G. Wen, *ibid* **43**, 11025 (1991); M. Stone, *Ann. Phys. (N.Y.)* **207**, 38 (1991).
- ²³ M. Stone, H. W. Wyld, and R. L. Shult, *Phys. Rev. B* **45**, 14156 (1992); U. Zulicke and A. H. MacDonald, *ibid* **54**, 16813 (1996); S. Giovanazzi, L. Pitaevskii, and S. Stringari, *Phys. Rev. Lett.* **72**, 3230 (1994).
- ²⁴ O. G. Balev and P. Vasilopoulos, *Phys. Rev. Lett.* **81**, 1481 (1998); O.G. Balev, P. Vasilopoulos, and Nelson Studart, *J. Phys.: Condens. Matter* **11**, 5143 (1999); O. G. Balev and P. Vasilopoulos, *Phys. Rev. B* **56**, 13252 (1997).
- ²⁵ O. G. Balev and Nelson Studart, *Phys. Rev. B* **61**, 2703 (2000); Sanderson Silva and O. G. Balev, *J. Appl. Phys.* **107**, 104310 (2010); I.O. Baleva, N. Studart, and O.G. Balev, *Phys. Rev. B* **65**, 073305 (2002).
- ²⁶ O. G. Balev and P. Vasilopoulos, *Phys. Rev. B* **59**, 2807 (1999).
- ²⁷ O. G. Balev, Nelson Studart, and P. Vasilopoulos, *Phys. Rev. B* **62**, 15834 (2000).
- ²⁸ R. C. Ashoori, H. L. Stormer, L. N. Pfeiffer, K. W. Baldwin, and K. West, *Phys. Rev. B* **45**, 3894 (1992).
- ²⁹ G. Ernst, R. J. Haug, J. Kuhl, K. von Klitzing, and K. Eberl, *Phys. Rev. Lett.* **77**, 4245 (1996).
- ³⁰ M. N. Khannanov, A. A. Fortunatov, and I. V. Kukushkin,

- Pis'ma Zh. Eksp. Teor. Fiz. **90**, 740 (2009) [JETP Lett. **90**, 667 (2009)].
- ³¹ V. Lukose, R. Shankar, and G. Baskaran, Phys. Rev. Lett. **98**, 116802 (2007).
- ³² N. M. R. Peres and E. V. Castro, J. Phys. Condens. Matter **19**, 406231 (2007).
- ³³ C. W. J. Beenakker and H. van Houten, in *Quantum Transport in Semiconductor Nanostructures*, Solid State Physics Vol. 44 edited by H. Ehrenreich and D. Turnbull (Academic, San Diego, 1991).
- ³⁴ D. J. Thouless, Phys. Rev. Lett. **71**, 1879 (1993).
- ³⁵ O. G. Balev and P. Vasilopoulos, Phys. Rev. B **54**, 4863 (1996).
- ³⁶ Y. Zheng and T. Ando, Phys. Rev. B **65**, 245420 (2002); V. P. Gusynin and S. G. Sharapov, Phys. Rev. Lett. **95**, 146801 (2005).
- ³⁷ O. G. Balev, F. T. Vasko, and V. Ryzhii, Phys. Rev. B **79**, 165432 (2009).
- ³⁸ A. H. MacDonald, T. M. Rice, and W. F. Brinkman, Phys. Rev. B **28**, 3648 (1983).
- ³⁹ D. J. Thouless, J. Phys. C **18**, 6211 (1985).